10-1991

Vorticity Dynamics of Seasonal Variations of the Antarctic Circumpolar Current from a Modeling Study

John M. Klinck
Old Dominion University, jklinck@odu.edu

Vorticity Dynamics of Seasonal Variations of the Antarctic Circumpolar Current from a Modeling Study

JOHN M. KLINCK

Department of Oceanography, Old Dominion University, Norfolk, Virginia

ABSTRACT

A one-layer numerical model was developed to analyze the vorticity dynamics of the seasonal variations of currents in the Southern Ocean. The model includes the continental geometry and bathymetry of the Southern Ocean and is forced by monthly climatological wind stress. Five cases are considered that compare (i) circulation over a flat bottom to that with bathymetry, (ii) effects of zonally averaged wind stress forcing versus the climatological forcing and (iii) anomaly wind stress (winds with the annual mean removed) versus the full stress. The individual terms in the vorticity conservation equation are calculated from the model solution along two latitude lines; 57.5°S, which passes through Drake Passage, and 43.5°S, which is in the subtropical gyres. In the zonal part of the flat bottom simulation, the curl of the surface stress balances bottom stress curl. However, in Drake Passage, beta (advection of planetary vorticity) balances bottom loss—the western boundary balance. Such vorticity interactions depend on the partial barrier of South America and, thus, do not occur in zonal channel models. The removal of vorticity occurs throughout the Southern Ocean for the seasonally varying winds but the mean circulation is balanced mainly by losses near Drake Passage. The location of the Antarctic Circumpolar Current (ACC) is controlled by the tip of South America rather than the structure of the wind. The seasonal changes in the model surface elevation in Drake Passage occur largely in the southern part of the passage, in agreement with pressure observations. The calculated ACC transport is similar for climatological and zonally averaged winds but the structure of the forced circulation is rather different for the two cases. Bottom topography changes the vorticity interactions so that the largest effects occur where the flow is forced over bathymetry creating relative vorticity by stretching, which is then removed by bottom friction. The major loss in the model occurs near Drake Passage, although there are smaller losses at other locations along 57.5°S. Bathymetry provides a strong counterforce to the wind stress and the transport is reduced by a factor of ten compared to the comparable uniform depth simulation. Friction plays a secondary role by determining the width of the currents and the spinup time but has only a weak effect on the total transport.

1. Introduction

The dynamics of the Antarctic Circumpolar Current (ACC) has been studied since the early 1950s but the dynamical balances that explain circulation in subtropical gyres are inappropriate in the Southern Ocean because of the apparent zonal nature of the ACC. The forcing mechanism for the ACC is clearly the strong westerly winds. What remains to be determined is how the seasonally varying wind stress forces the circulation of the ACC and what mechanism(s) balance the forcing. A number of dynamical processes have been proposed (for a review see Nowlin and Klinck 1986), including small-scale friction, mesoscale eddy and bottom topography effects, as dissipative mechanisms for the energy put into the ACC by the winds.

The only substantial observations on the seasonal variation of the ACC are the direct measurements of transport in Drake Passage between 1977 and 1982

(Whitworth and Peterson 1985). The general picture that emerges from these measurements is that the transport has a semiannual variation with the largest transports tending to occur in spring and fall. However, there is considerable interannual variability so the peak transport can occur in almost any month. In three of the five years, the largest transport occurred during the southern spring.

The seasonal variability of the Southern Hemisphere winds has been explained (van Loon 1971; Large and van Loon 1989) in terms of the annual and semiannual variations of the atmospheric temperature and pressure in the Southern Hemisphere. A comparison between winds and the speed of surface drifters during the FGGE experiment show that they are related at a semiannual period (Large and van Loon 1989).

Altitude observations from Geosat (Chelton et al. 1990) are used to analyze sea surface variations over wide areas for long time spans. The lack of a good geoid limits the use of altimetry to the study of variability rather than mean structure. Twenty-six months of observations were subjected to an EOF analysis revealing that variations occur at annual and semiannual

Corresponding author address: John M. Klinck, Department of Oceanography, Old Dominion University, Norfolk, VA 23529.

periods and that the ACC varies regionally rather than as a monolithic current.

The dynamics of the large spatial scale variations in the circulation of the Southern Ocean has been considered by Clarke (1982), who reveals that there are two different time scales for the variability of the flow in this region. The slowest changes occur over time scales greater than 70 years and are associated with the redistribution of density. In contrast, the barotropic variations, which are due to changes in the shape of the free surface, can occur on time scales of approximately a week. Therefore, the seasonal variations in the large-scale structure of the Southern Ocean occur through a barotropic process.

Eddies that result from baroclinic instability of the ACC are known to play a role in heat and momentum fluxes in the Southern Ocean (Joyce 1977; McWilliams et al. 1978; Johnson and Bryden 1989; Wolff and Olbers 1989; Treguier and McWilliams 1990). These eddy processes occur over time scales of one to two months, in contrast to the baroclinic time scale of one century given above. However, the cumulative effect of the eddies is the important issue and the changes in eddy fluxes appear to occur slowly. In large-scale ocean models, these eddy effects are usually represented by eddy diffusivities, even though these closure hypotheses may not always be correct. Eddy-resolving models are needed to clarify the role of eddies in the Southern Ocean.

The most often mentioned process for removal of energy from the ACC is bottom form drag. The earliest calculation (Munk and Palmén 1951) revealed that modest pressure differences (a few dynamic centimeters) across the largest-scale topography in the Southern Ocean produce sufficient drag to balance the surface wind stress. A one-layer model of the ACC (Schulman 1975) reinforced this conclusion by showing that the addition of bathymetry in the vicinity of Drake Passage was sufficient to reduce the transport of the ACC by a factor of ten. Studies of the interaction of zonal jets with submarine ridges (Hogg 1980; Pratt 1989) also indicate the strong effect of topography on oceanic jets. The most important effect may be the production of standing eddies (circulation patterns created by bottom topography), which cause semipermanent distortions of the isopycnal surfaces, and therefrom, an internal form drag (Treguier and McWilliams 1990).

An unanswered question with regard to wind-driven circulation in the Southern Ocean is the relation of the circulation to the Sverdrup balance. Several calculations show a correspondence between the Sverdrup transport across the latitude of the tip of South America and the transport through Drake Passage (e.g., Wyrtki 1960; Baker 1982). Furthermore, the pressure at 500 m depth in Drake Passage is correlated with the zonal average of the curl of the wind stress in latitude bands on either side of the passage (Peterson 1988). However, Clarke (1982) argues from an analytical solution that the ACC is not in a Sverdrup balance with the seasonally varying winds.

The purpose of this paper is to consider the vorticity interactions in a simplified (one-layer) wind-driven model of the Southern Ocean. Since the seasonal variability of the ACC is barotropic, the simplest model that describes the circulation has vertically averaged dynamics (the shallow water equations). The geometry and bathymetry of the Southern Ocean are included in the model and the simulated circulation is obtained by forcing with climatological winds. Since the model has only one layer, mesoscale eddies are not allowed in the solution. The effect of eddies is represented as a subgrid-scale process through the use of eddy viscosities. The circulation obtained from the model is analyzed by calculating the terms in the vorticity equation, which provides an estimate of the magnitude of the various processes contributing to the circulation.

Section 2 describes the numerical model and the vorticity equation that is evaluated. Section 3 discusses five cases that are used to analyze the vorticity interactions. Section 4 compares the simulations and shows how the results relate to earlier theoretical and numerical studies. The last section summarizes the results of this paper.

2. Model formulation

a. Model geometry

The model domain (Fig. 1) extends from the Antarctic continent to the northern boundary of the southern subtropical gyres, encompassing the region from 75° to 25°S. The domain is chosen to extend far enough north to include most of the subtropical gyres, thus insulating the ACC from the influence of the northern model boundary. This inclusion of most of the subtropical gyres allows the location of the ACC to be determined by the wind forcing and bottom topography rather than by an artificial constraint imposed by the model boundaries. Furthermore, the larger model domain allows Africa, New Zealand, and Australia to be represented in addition to South America.

The bathymetry for the model domain (Fig. 1) is obtained from data on a 1° × 1° grid compiled by Gates and Nelson (1975) and distributed by NCAR. The zero depth contour from this bathymetry dataset defines the continental boundaries appropriate for the grid resolution chosen for the finite difference model. Because the model uses a spatially staggered grid (discussed below), some minor adjustment of the location of continental boundaries is needed for the walls to occur at the appropriate variable (that is, zonal walls on v variables and meridional walls on u variables). The bathymetry is smoothed by three passes of a 5-point smoother in order to match the resolution of the model. Furthermore, the depth was constrained to be at least 100 m deep to avoid erroneously high forcing near the coast.
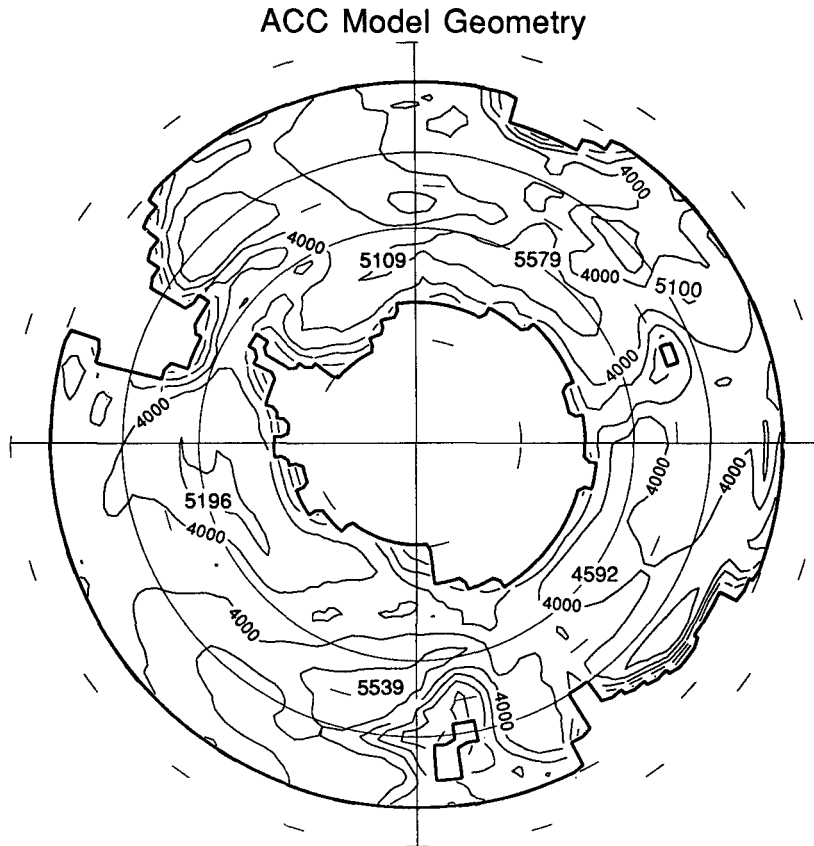
ACC Model Geometry

FIG. 1. Domain and bottom topography for the one-layer model. The active domain is 25°
to 75°S and the continental boundaries are indicated by heavy lines. The two circular lines
denote two latitudes along which the vorticity has been calculated (57.5° and 43.5°S). The
lighter lines are depth contours in meters and the contour interval is 1000 m. The 4000-m
contour is labeled and the numbers are maximum depths in meters.

b. Wind data

The climatological (monthly) wind stress, on a 2.5°
× 2.5° grid prepared by Trenberth et al. (1989), is
used to force the circulation. The simulations discussed
here are forced either by the monthly wind stress or
the monthly wind stress minus the annual mean. In
some cases, these fields are averaged zonally. Seasonally
varying winds were then constructed from the monthly
winds by interpolation to each model time step.

The general structure of the time variability of the
wind forcing is indicated in the zonal average of the
monthly climatological eastward wind stress (Fig. 2).
Over the northern part of the model domain (25° to
45°S), the variability has an annual character while
that over the southern part (55° to 75°S) is semiannual.
The eastward wind stress is largest in the spring and
fall, smallest in the summer and winter. The temporal
behavior of the winds at different latitudes, which pro-
duces this structure, is discussed elsewhere (van Loon
1971; Large and van Loon 1989).

The quality of wind climatology over the Southern
Ocean has been called into question due to a lack of

sufficient observations in this remote region. Since the
ACC transport seems to respond most strongly to the
zonally integrated wind stress (Clarke 1982), the errors
will average out to some extent. In any case, the issue
of concern here is the vorticity dynamics that is active
as the ACC is forced by the seasonally varying winds.
Earlier simulations for this study used the Hellerman
and Rosenstein (1983) winds, which lead to generally
the same results as presented here, although the winds
were a little weaker and the model solutions were cor-
respondingly weaker. The vorticity analyses did not
differ substantially for the two different wind clima-
tologies. Therefore, the winds will be taken to be of
adequate quality for this vorticity consideration.

c. Model equations and numerical procedure

The governing equations for this model are the ver-
tically averaged primitive equations with a free surface
in a periodic β-plane zonal channel. The primitive
equations are used rather than those based on the quasi-
geostrophic assumption since the latter demand that
the integrated eastward transport in a zonal channel
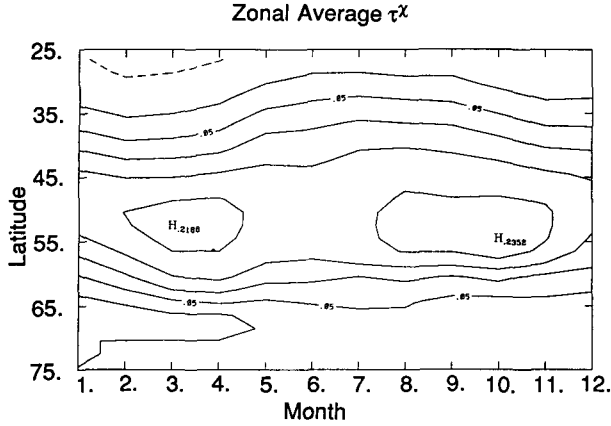
Zonal Average τ^x

FIG. 2. Zonally average eastward wind stress (Trenberth et al. 1989) as a function of latitude and month. Only the points over the ocean are included in the zonal average. The dashed contours indicate negative values and the contour interval is 0.05 N m^{-2}. Maximum values are marked.

be identical at every longitude since the northern and southern boundaries are streamlines. The governing equations for the horizontal velocity components (u, v) (eastward and northward, respectively) and the surface elevation (η) are

$$\frac{D}{Dt} u = +fv - g\frac{\partial \eta}{\partial x} - ru + A\nabla^2 u + \frac{\tau^x}{\rho_0 h}, \quad (1)$$

$$\frac{D}{Dt} v = -fu - g\frac{\partial \eta}{\partial y} - rv + A\nabla^2 v + \frac{\tau^y}{\rho_0 h}, \quad (2)$$

$$\frac{\partial}{\partial t} \eta = -\frac{\partial}{\partial x}(hu) - \frac{\partial}{\partial y}(hv), \quad (3)$$

$$\frac{D}{Dt} = \frac{\partial}{\partial t} + u\frac{\partial}{\partial x} + v\frac{\partial}{\partial y},$$

where $h = H - \eta_b$ is the mean water thickness and $f = f_0 + \beta y$, representing a linear variation of the Coriolis parameter over the basin. The parameters in the model are gravity (g), mean depth (H), rotation (f_0 and β), a reference density (ρ_0), linear friction (r), lateral friction (A), and bathymetry (η_b). The linear loss term represents a number of drag forces including bottom friction, wave drag, or other processes that tend to retard the geostrophic flow (Clarke 1982). In the text, this process may be referred to as bottom friction, which it is in a general sense.

The inclusion of a free surface permits the fast external gravity wave, which severely limits the maximum time step in the numerical model. This restriction is avoided by using an alternating direction implicit (ADI) scheme (Leendertse 1967). The general time-stepping procedure involves two parts. During the first step the gravity wave terms in the x momentum equation and the x derivative in the divergence equation

are evaluated implicitly (at the new time level) and the remainder of the terms are evaluated explicitly (at the old time level). In the second step, the gravity wave terms in the y momentum equation and the y derivative term in the divergence equation are evaluated implicitly. The following time-differenced equations illustrate the scheme.

x sweep:

$$u^{n+1} - u^n = -g\Delta t\partial_x\eta^{n+1} + F_u{}^n$$

$$v^{n+1} - v^n = -g\Delta t\partial_y\eta^n + F_v{}^n$$

$$\eta^{n+1} - \eta^n = -\Delta t\partial_x[(H - \eta_b)u^{n+1}]$$
$$- \Delta t\partial_y[(H - \eta_b)v^n] + F_\eta{}^n \quad (4)$$

y sweep:

$$u^{n+2} - u^{n+1} = -g\Delta t\partial_x\eta^{n+1} + F_u{}^{n+1}$$

$$v^{n+2} - v^{n+1} = -g\Delta t\partial_y\eta^{n+2} + F_v{}^{n+1}$$

$$\eta^{n+2} - \eta^{n+1} = -\Delta t\partial_x[(H - \eta_b)u^{n+1}]$$
$$- \Delta t\partial_y[(H - \eta_b)v^{n+2}] + F_\eta{}^{n+1} \quad (5)$$

where F represents the other terms in each of the equations (the subscript indicates which equation), the superscript gives the time level of the variable, and ∂ is a partial derivative with respect to the subscript.

The benefit of this two-step procedure is that the scheme exhibits unconditional stability for the external gravity wave while only requiring that a set of linear equations with a tridiagonal coefficient matrix be solved at each time step. For a fully implicit integration scheme, a time-consuming, two-dimensional elliptic solver must be used at each time step. Efficient elliptic solvers exist but they usually require regular geometry, which is not the case for this Southern Ocean calculation. The time step for all of the simulations presented below is one hour.

The model variables are arranged on a spatially staggered grid such that the eastward velocity component (u) is one grid interval east and west of an elevation (η) point while the northward velocity component (v) is one grid interval north and south of the elevation point (a C grid, Mesinger and Arakawa 1976). Spatial derivatives are represented by second-order accurate central differences.

After-the-fact masking of the variables to remove land points does not work in this ADI scheme since all variables along a line affect the solution. The proper procedure is to change the linear equations along each grid line such that the masked points are set to zero. This modification involves changing the coefficients of the tridiagonal system corresponding to every velocity grid point over land; the diagonal coefficient is set to one, the off-diagonal coefficients and the forcing are set to zero, thus forcing the new values to be zero. A masking array containing zeros and ones is used in this operation so that water and land points within the

model domain are specified. The mask array is also used to control the calculation of stress at the walls.

d. Parameter choices

All but two of the parameters for this set of simulations are easily determined. The mean depth (H = 3892 m) is obtained by averaging the depth in the model domain (Fig. 1). The central latitude of the β plane is chosen to be 55°S, which determines the values of the Coriolis (f_0) and β parameters as -1.194×10^{-4} s^{-1} and 1.31×10^{-11} m^{-1} s^{-1}. The gravitational acceleration (g) is 9.8 m s^{-2} and the base density (ρ_0) is 1000 kg m^{-3}.

The two poorly known parameters in this model are linear damping (r) and lateral eddy viscocity (A). Each of these parameters represents a variety of processes making it difficult to estimate the appropriate values. The linear friction process represents drag that results from Ekman suction, wave drag, and form drag at the bottom of the ocean. There is an extended discussion of these processes for the Southern Ocean in Clarke (1982) and values in the range of 10^{-6} to 10^{-7} s^{-1} [which result in a spindown time ($1/r$) of 10 to 20 days] are obtained. The lateral friction parameter is equally difficult to estimate and a variety of values in the range of 10^2 to 10^4 m^2 s^{-1} are considered appropriate (Gill 1982, p. 518).

The friction parameters constrain the choice of grid spacing since the thicker of the two possible viscous boundary layers must be resolved. The grid resolution of the model discussed here is approximately 2° of longitude (128 km at 55°S), which gives the minimum values of the linear and lateral friction parameters as 1.8×10^{-6} s^{-1} and 2×10^4 m^2 s^{-1}, which are at the upper end of the range of acceptable values. However, the linear spindown time is about 6 days, which is about correct for the Southern Ocean; the lateral viscosity is comparable to values used in the large-scale, low-resolution general circulation models for the ocean (Bryan and Cox 1972). For simulations presented here, linear friction is chosen to dominate while lateral friction is reduced by a factor of 100, so its effect is minimized. This choice allows the simulations to be compared to previous analytical calculations by Gill (1968). The frictional parameters used in all of the simulations discussed here are $r = 2 \times 10^{-6}$ s^{-1} and $A = 2 \times 10^2$ m^2 s^{-1}.

e. Vorticity equation

There are two general forms of the vorticity equation: vertically averaged vorticity and vertically integrated vorticity. The conservation equation for the vertically averaged vorticity is obtained from the curl of the vertically averaged momentum equations; for the vertically integrated vorticity, the momentum equations are first multiplied by the depth ($h = H - \eta_b$) and then the curl operation is performed. This second equation

is preferred for this analysis since the bottom torque will appear explicitly.

On multiplying (1) and (2) by the depth and cross differentiating, one obtains the following depth-integrated vorticity equation:

$$
\frac{\partial}{\partial t}\left(\frac{\partial(hv)}{\partial x} - \frac{\partial(hu)}{\partial y}\right) + \beta hv + f\left(\frac{\partial(hu)}{\partial x} + \frac{\partial(hv)}{\partial y}\right)
$$

$$
+ g\left(\frac{\partial}{\partial x}\left(h\frac{\partial\eta}{\partial y}\right) - \frac{\partial}{\partial y}\left(h\frac{\partial\eta}{\partial x}\right)\right)
$$

$$
+ r\left(\frac{\partial(hv)}{\partial x} - \frac{\partial(hu)}{\partial y}\right) - A\left(\frac{\partial}{\partial x}(h\nabla^2 v)\right)
$$

$$
- \frac{\partial}{\partial y}(h\nabla^2 u)\right) + \frac{\partial}{\partial x}\left(hu\frac{\partial v}{\partial x}\right) - \frac{\partial}{\partial y}\left(hu\frac{\partial u}{\partial x}\right)
$$

$$
+ \frac{\partial}{\partial x}\left(hv\frac{\partial v}{\partial y}\right) - \frac{\partial}{\partial y}\left(hv\frac{\partial u}{\partial y}\right)
$$

$$
- \frac{1}{\rho_0}\left(\frac{\partial \tau^y}{\partial x} - \frac{\partial \tau^x}{\partial y}\right) = 0. \quad (6)
$$

In the following discussion, the terms in this equation are referred to as time difference, beta, stretching, bottom torque, bottom loss, lateral loss, u advection, v advection, and wind curl, respectively.

Vorticity interactions are analyzed by evaluating each term in this equation along a line of constant latitude. To ensure that there were no problems with the model or the vorticity calculation, the sum of these terms was calculated along with the individual terms. The maximum absolute value of the residual was typically 1% to 10% of the maximum of all the terms while the rms of the residual was always at least an order of magnitude less than the maximum residual. In general, the flat-bottom, zonally averaged wind-forced simulations had the smallest maximum residual while the full-topography, climatological wind-forced simulations had the largest.

The simulations considered here had negligible contribution from the nonlinear advection terms and from the lateral viscosity term, so none of these terms nor the error will be displayed in this paper.

3. Results

The focus of this paper is the vorticity dynamics of the ACC and the contrast of these dynamics with the vorticity interactions in a subtropical gyre—which are better understood; therefore, five cases are examined in detail. The first three cases look at the effect of different wind patterns on a Southern Ocean with uniform depth. Case I is forced by the zonal average of the monthly winds, while case II is forced by the zonal average of the monthly anomaly winds (monthly winds minus the annual mean). Case III is forced by the full structure of the monthly winds. The first two cases

contrast the vorticity processes for an ocean with and without a time-mean circulation. The third case looks at the influence of longitudinally varying wind stress curl. The last two cases consider the circulation in the Southern Ocean with the bathymetry appropriate for the model resolution. Case IV is forced by the zonal average of monthly winds, and case V is forced by the zonal average of the monthly anomaly winds. These cases examine the effect of bottom topography on the vorticity dynamics for circulation with and without a time mean flow.

a. Case I: Flat bottom with zonally averaged monthly wind stress

This case considers the effect of continental boundaries and the average structure of the wind stress on the vorticity dynamics of the ACC. It should compare most closely to the various analytical, periodic channel models that have been used to analyze the dynamics of the ACC (e.g., Gill 1968), except that this case has realistic wind stress and continental geometry.

The model simulation begins at a state of rest and the model is run for one year with the results saved every month (730 steps). A spinup time of one month is evident in the transport at Drake Passage (Fig. 3a). The eastward transport is calculated at three other locations (south of Africa, south of Tasmania, south of New Zealand) and each of these time series is identical to that at Drake Passage. The annual mean transport is about 180 Sv ($1 \text{ Sv} \equiv 1 \times 10^6 \text{ m}^3 \text{ s}^{-1}$) and there is a semiannual variation with an amplitude of about 20 Sv. The largest transport occurs in the spring and fall; the smallest transport is in the summer with a secondary minimum occurring in the winter.

The surface elevation at the Greenwich meridian (Fig. 3b) indicates a persistent ACC with a surface elevation change across the current of about 40 cm. The semiannual increase of the surface gradient in the spring and fall corresponds to a stronger ACC. Note also that there is no latitudinal shift in the location of the ACC as the transport changes strength. The semiannual variation of the Weddell gyre is also evident. The surface elevation across Drake Passage (Fig. 3c) has a similar mean surface slope and a semiannual variation. However, the surface elevation in Drake Passage changes only in the south; the surface elevation is effectively constant in the northern passage. Peterson (1988) found that the seasonal variation in bottom pressure due to wind forcing occurred almost exclusively on the southern side of the passage.

The largest terms in the vorticity equation are displayed along two latitude lines: 57.5°S (Fig. 4a,b), which passes through Drake Passage, and 43.5°S (Fig. 4c), which passes through the subtropical gyres (each of these latitude lines is shown on Fig. 1). The vorticity advection and the lateral friction terms are smaller than the rms error of the calculation and are not displayed.
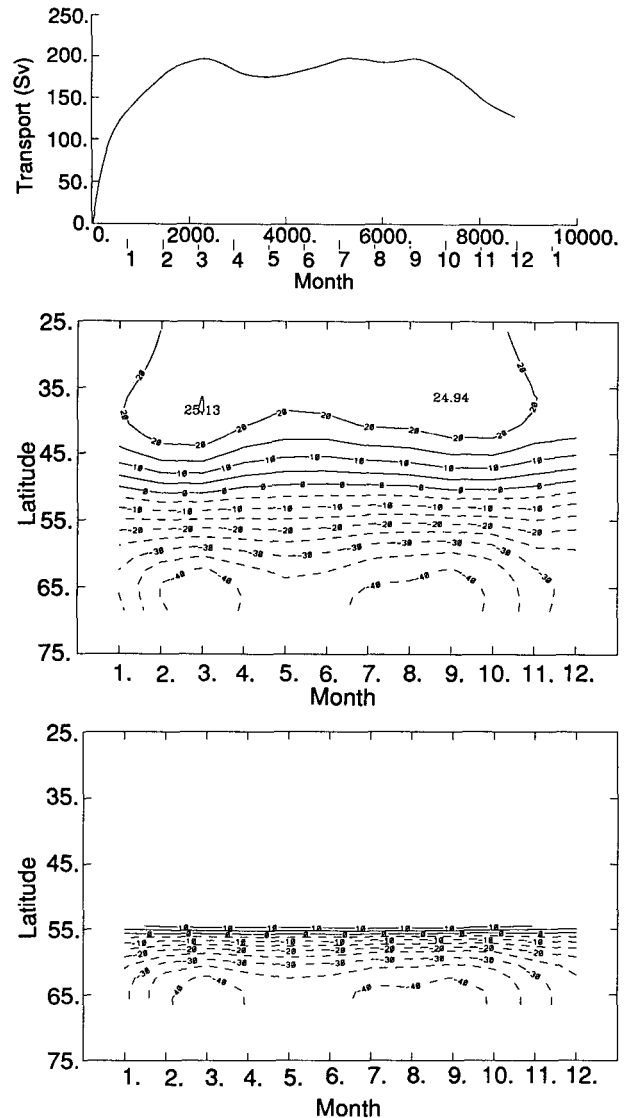

FIG. 3. Total transport and surface elevation changes for case I, which has a flat bottom and is forced by the zonal average of the monthly winds. The simulation begins at a state of rest. (a) The total transport for the first year of the simulation as a function of time. Both time step and month are indicated. The monthly tics indicate the beginning of the month. The ordinate has units 1 Sv = 1 × 10⁶ m³ s⁻¹. (b) The variation of the surface elevation (cm) at the Greenwich meridian by month on the abscissa and latitude on the ordinate. The contour interval is 5 cm and the maximum values are marked. Dashed lines indicate negative values. (c) The variation of the surface elevation (cm) across Drake Passage by month on the abscissa and latitude on the ordinate. The contour interval is 5 cm. Dashed lines indicate negative values.

Along 57.5°S, the vorticity terms are shown at two times: step 3650 (after five months of simulation), at which point the transport is at a relative minimum and step 5110 (after seven months of simulation), at which the transport is at a maximum. The analysis at 43.5°S is shown only at step 3650, since the vorticity processes

Vorticity equation

Latitude = -57.50S   Time = 166.7 days
JNDEX = 10   TIME STEP = 3650

Vorticity equation

Latitude = -57.50S   Time = 227.5 days
JNDEX = 10   TIME STEP = 5110

Vorticity equation

Latitude = -43.50S   Time = 166.7 days
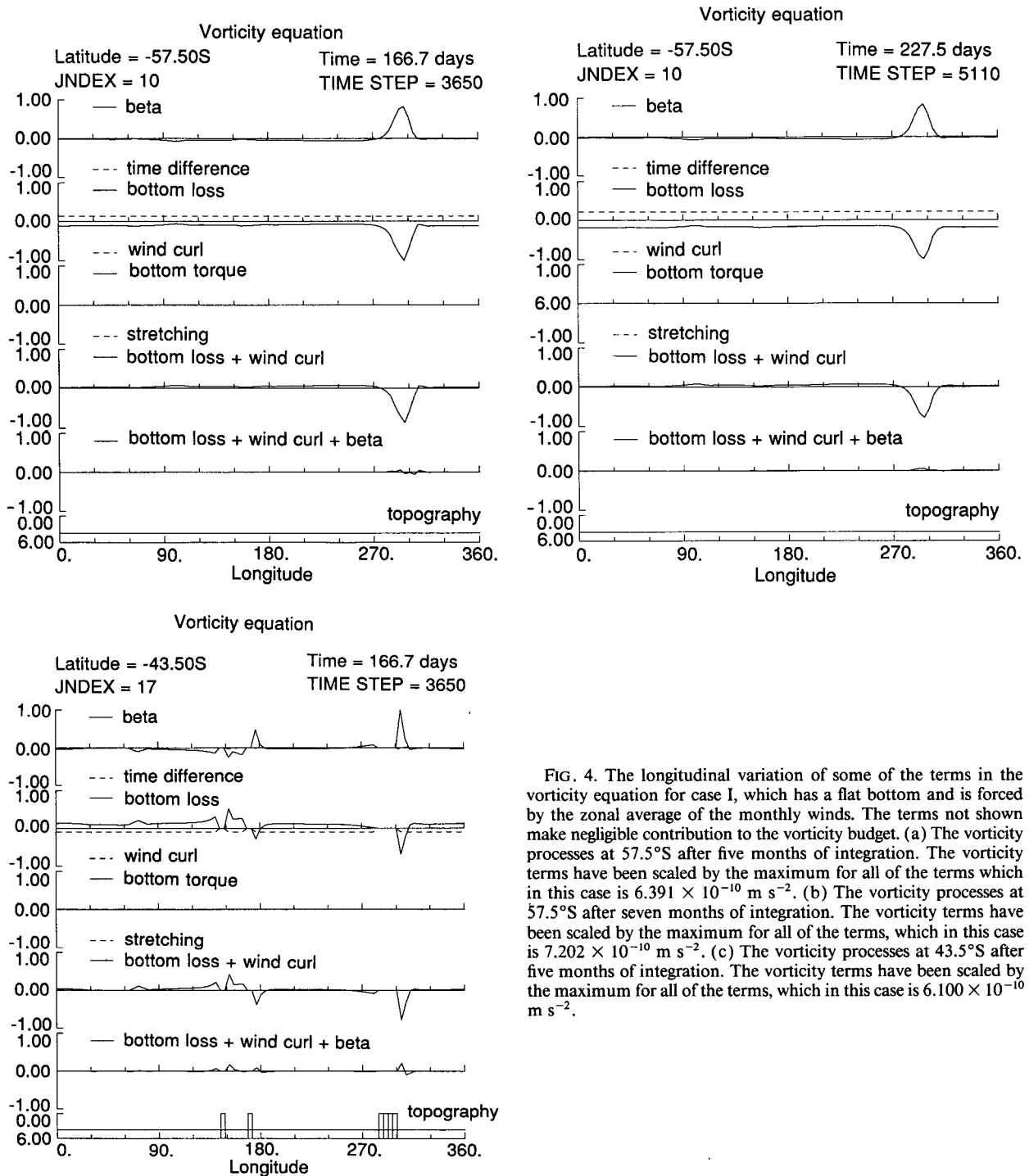JNDEX = 17   TIME STEP = 3650

FIG. 4. The longitudinal variation of some of the terms in the vorticity equation for case I, which has a flat bottom and is forced by the zonal average of the monthly winds. The terms not shown make negligible contribution to the vorticity budget. (a) The vorticity processes at 57.5°S after five months of integration. The vorticity terms have been scaled by the maximum for all of the terms which in this case is 6.391×10^{-10} m s^{-2}. (b) The vorticity processes at 57.5°S after seven months of integration. The vorticity terms have been scaled by the maximum for all of the terms, which in this case is 7.202×10^{-10} m s^{-2}. (c) The vorticity processes at 43.5°S after five months of integration. The vorticity terms have been scaled by the maximum for all of the terms, which in this case is 6.100×10^{-10} m s^{-2}.

are the same for all times after the initial spinup transients. The vorticity terms in each figure have been normalized by a constant (given in the figure legend), which is approximately the same for figures pertaining to the same case.

In the zonal part of the channel and away from Drake Passage (Fig. 4a), the two largest terms are bot-tom loss and wind curl, which are approximately equal and of opposite sign. The wind curl adds negative vorticity to the flow while bottom friction removes negative vorticity. This inverse relationship is easy to see from the fourth panel in Fig. 4a, which is the sum of these two terms. If the balance were that of a zonal channel (e.g., section 3d in Clarke 1982), then the only other

term to contribute would be the time derivative term but it is clear from the top panel in Fig. 4a that time changes of vorticity are negligible. The largest contributions to the vorticity equation occur in the vicinity of Drake Passage (70°W or 290° in Fig. 4a) where the beta term creates negative vorticity, which is removed by bottom loss—the classical Stommel western boundary balance.

There is a small positive residue in the sum of the bottom loss and wind curl terms (fourth panel, Fig. 4a) that is balanced by a small negative value in the beta term indicating a Sverdrup balance. Furthermore, these terms decrease approximately linearly to the west as expected.

The three active processes for this circumpolar channel are clearly wind curl, beta, and bottom friction, as can be seen by the small size of the sum of these processes (fifth panel, Fig. 4a). There are three general balances that are indicated: a surface forcing to bottom loss balance, a Sverdrup interior (Pacific sector), and a western boundary balance near the tip of South America. Note that a majority of the frictional loss along this latitude occurs near Drake Passage and in the Scotia Sea.

After seven months of simulation, the vorticity balances (Fig. 4b) are basically the same as discussed above. The wind curl is stronger and the scale factor is slightly larger (7.2 × 10⁻¹⁰ versus 6.4 × 10⁻¹⁰) but the three major terms are still wind curl, beta, and bottom loss (fifth panel, Fig. 4b). Furthermore, the relative magnitudes of the three processes are the same as at the previous time.

The midlatitude part of the model simulation (Fig. 4c) after 3650 time steps has a rather different character from that at 57.5°S, although the same three vorticity processes are important. The dissipation in the western boundary is not the major loss at this latitude as it was along the zonal part of the model. The wind curl is more nearly balanced by bottom loss except near the eastern sides of the ocean basins where beta balances the wind curl. There is a pronounced western boundary balance on each of the ocean walls. Note, however, that the boundary currents along South America and New Zealand flow northward while that along Australia flows to the south.

b. Case II: Flat bottom with zonally averaged anomaly wind stress

The zonally averaged monthly winds minus the annual mean forces the circulation so there will be no mean circulation. Therefore, the vorticity processes responsible for the seasonal changes will be more clearly displayed.

The transport at Drake Passage (Fig. 5a) varies from −40 to 20 Sv with the largest transport in the spring and fall; the variation is the same as for the previous case (Fig. 3a). The surface elevation at the Greenwich
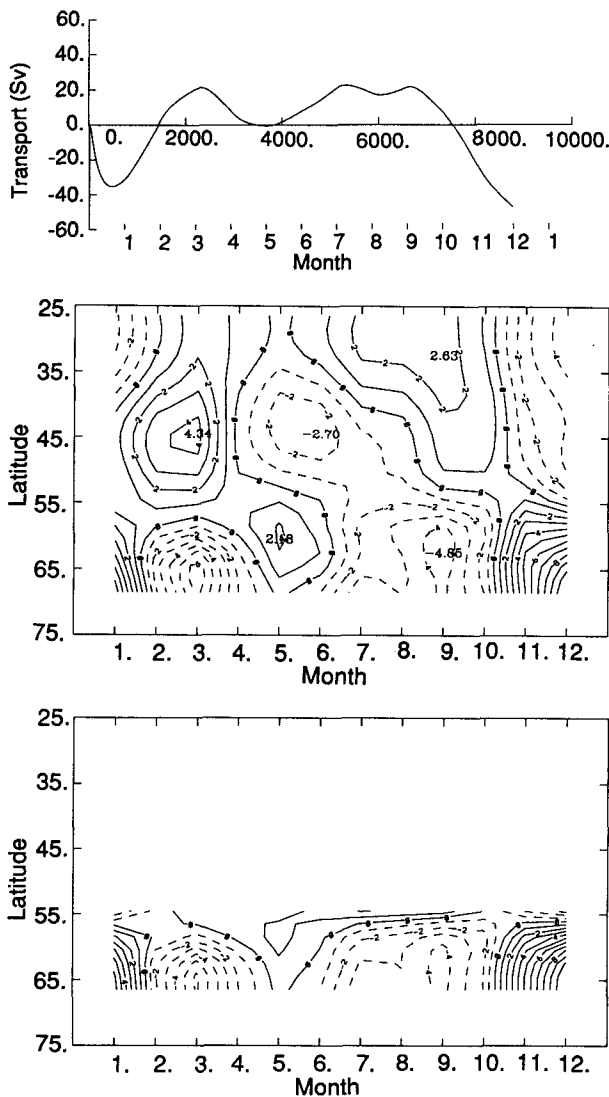

FIG. 5. Total transport and surface elevation changes for case II, which has a flat bottom and is forced by the zonal average of monthly winds minus the annual mean. The simulation begins at a state of rest. (a) The total transport for the first year of the simulation as a function of time. Both time step and month are indicated. The monthly tics indicate the beginning of the month. The ordinate has units 1 Sv = 1 × 10⁶ m³ s⁻¹. (b) The variation of the surface elevation (cm) at the Greenwich meridian by month on the abscissa and latitude on the ordinate. The contour interval is 1 cm and the maximum values are marked. Dashed lines indicate negative values. (c) The variation of the surface elevation (cm) across Drake Passage by month on the abscissa and latitude on the ordinate. The contour interval is 1 cm. Dashed lines indicate negative values.

meridian has a maximum difference of 8 cm with a semiannual variation (Fig. 5b). The surface topography pivots around 55°S, which confirms that there is little north–south shift in the location of the ACC. The variation of the surface topography in Drake Passage (Fig. 5c) reinforces the previous conclusion that the major changes are confined to the southern part of the passage. Annual period variations in the surface elevation occur

near the northern side of the passage. The node for this surface variation is near 55°S, which is the same as for the variations at the Greenwich meridian. The zero of the wind curl (estimated from Fig. 2) is near 52°S, so it is the tip of South America, not the zero wind-curl line, that determines the location of the ACC in the absence of bathymetry.

The vorticity processes at 57.5°S after five months of simulation (Fig. 6a) are an order of magnitude weaker than for the previous case (7.3×10^{-11} in Fig. 6a versus 6.4×10^{-10} in Fig. 4a), which is understandable since the mean wind curl has been removed. At this time the wind stress is at a minimum so the vorticity processes have an opposite sign from those shown
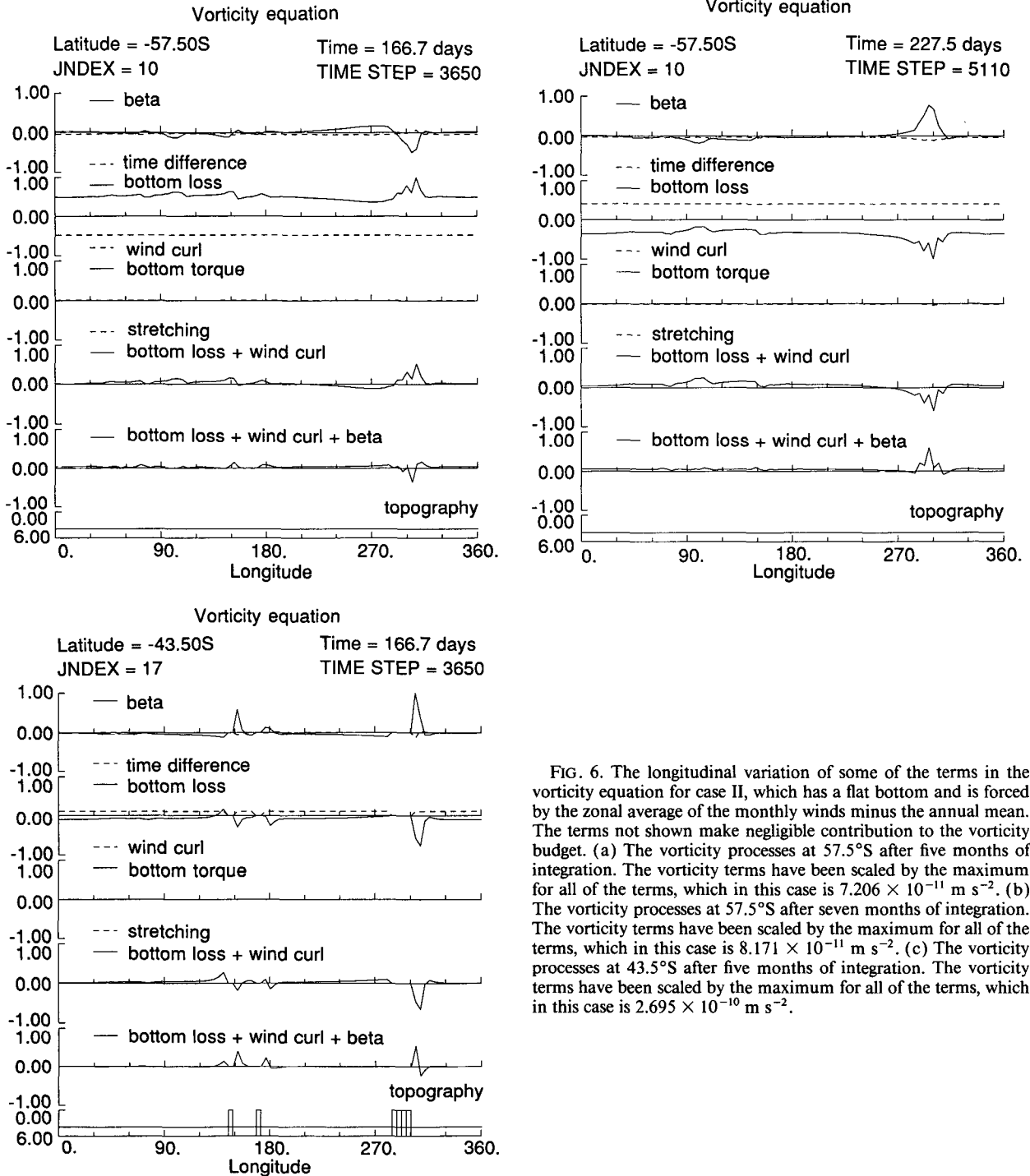

FIG. 6. The longitudinal variation of some of the terms in the vorticity equation for case II, which has a flat bottom and is forced by the zonal average of the monthly winds minus the annual mean. The terms not shown make negligible contribution to the vorticity budget. (a) The vorticity processes at 57.5°S after five months of integration. The vorticity terms have been scaled by the maximum for all of the terms, which in this case is 7.206×10^{-11} m s^{-2}. (b) The vorticity processes at 57.5°S after seven months of integration. The vorticity terms have been scaled by the maximum for all of the terms, which in this case is 8.171×10^{-11} m s^{-2}. (c) The vorticity processes at 43.5°S after five months of integration. The vorticity terms have been scaled by the maximum for all of the terms, which in this case is 2.695×10^{-10} m s^{-2}.

in Fig. 4a. The major vorticity processes are wind curl and bottom loss (second panel, Fig. 6a), the residual of which (fourth panel) is opposite to the beta term. The sum of the three largest terms (wind curl, beta, and bottom loss) is balanced by a small time derivative; the simulation is still adjusting slightly to the changing wind stress. The three major balances discussed before remain, except minor residual adjustment is now visible. In this case, the dissipation in the western boundary layer in Drake Passage is not the major loss mechanism; rather, loss occurs throughout the Southern Ocean.

After seven months of forcing (Fig. 6b), the wind curl has reversed (this is now the time of maximum wind forcing) and all of the vorticity processes have changed sign. Nevertheless, the relationship among the three major processes is the same as discussed above. Generally, wind curl is balanced by bottom loss. There is a western boundary balance in Drake Passage and a weak Sverdrup balance in the eastern Pacific Ocean. A small time change indicates that some adjustment is continuing.

At 43.5°S after five months of simulation (Fig. 6c) the vorticity processes are similar to those for case I (Fig. 4c). Wind curl and bottom loss balance is in the center of the gyres with a clear Sverdrup balance on the eastern side of the basins. All of the terms have changed sign except at Drake Passage; note that there is still a northward boundary current on South America in spite of the negative wind curl at this latitude. This boundary current is a continuation of the ACC along the coast of South America and it is importing positive vorticity from more southerly locations where the wind curl is positive (Fig. 6a). This sort of behavior is usually associated with nonlinear processes in closed basin models, but in this case the gap in the continents (Drake Passage) allows flow across the zero wind-curl line, even for a strictly linear flow. Since the wind curl at this latitude varies with an annual period, the corresponding figure after seven months of simulation is quite similar and is not shown.

c. Case III: Flat bottom with monthly anomaly wind stress

The forcing in this case is the monthly wind stress minus the annual mean; the results can be compared directly to those of case II to see the effect of longitudinally varying wind stress curl.

The transport at Drake Passage (Fig. 7a) is identical to that from case II (Fig. 5a), so it is the zonal integral of the wind that has the major effect on the transport of the ACC, at least for cases where the bottom topography is uniform. The difference between these two cases is evident in the surface elevation at the Greenwich meridian (Fig. 7b). North of 55°S, there is a semiannual oscillation of the free surface from +4 cm to −2 cm. However, south of 55°S, the surface eleva-
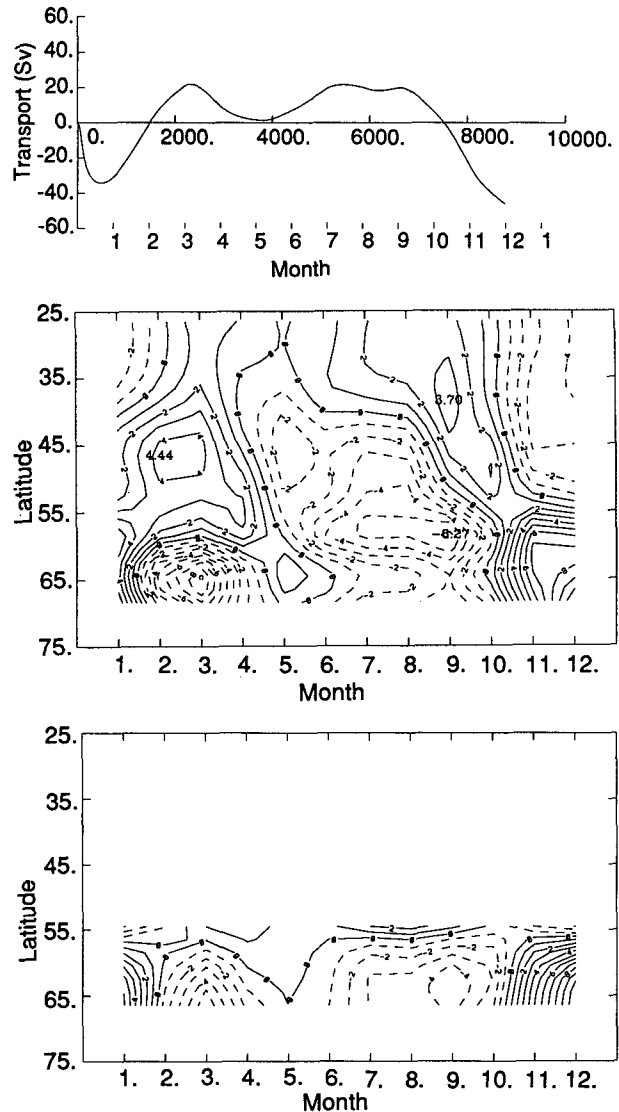

FIG. 7. Total transport and surface elevation changes for case III, which has a flat bottom and is forced by the monthly winds. The simulation begins at a state of rest. (a) The total transport for the first year of the simulation as a function of time. Both time step and month are indicated. The monthly tics indicate the beginning of the month. The ordinate has units 1 Sv $= 1 \times 10^6$ m^3 s^{-1}. (b) The variation of the surface elevation (cm) at the Greenwich meridian by month on the abscissa and latitude on the ordinate. The contour interval is 1 cm and the maximum values are marked. Dashed lines indicate negative values. (c) The variation of the surface elevation (cm) across Drake Passage by month on the abscissa and latitude on the ordinate. The contour interval is 1 cm. Dashed lines indicate negative values.

tion changes are much larger, from −8 cm to +1 cm; that is, the Weddell gyre is much stronger in this case where the winds are not zonally averaged. However, these differences are strictly local to the South Atlantic Ocean; the structure of the surface elevation in Drake Passage (Fig. 7c) is similar to the zonally averaged case

(Fig. 5c) with the largest changes occurring in the southern part of the passage and only minor annual variations in the northern part.

At 57.5°S after five months of simulation (Fig. 8a), the wind curl is spatially variable but mainly negative in the Pacific and Indian sectors while it is positive in the Atlantic sector. During this time the wind stress is at a minimum so the circulation is decelerating. In spite of the variability, there is a general anticorrelation between wind curl and bottom loss (Fig. 8a, second panel). The Sverdrup balance is also active as indicated by the residual of the wind curl and bottom loss terms (fourth panel) with the beta term (first panel). The Pacific and Indian ocean sectors display a clear inter-
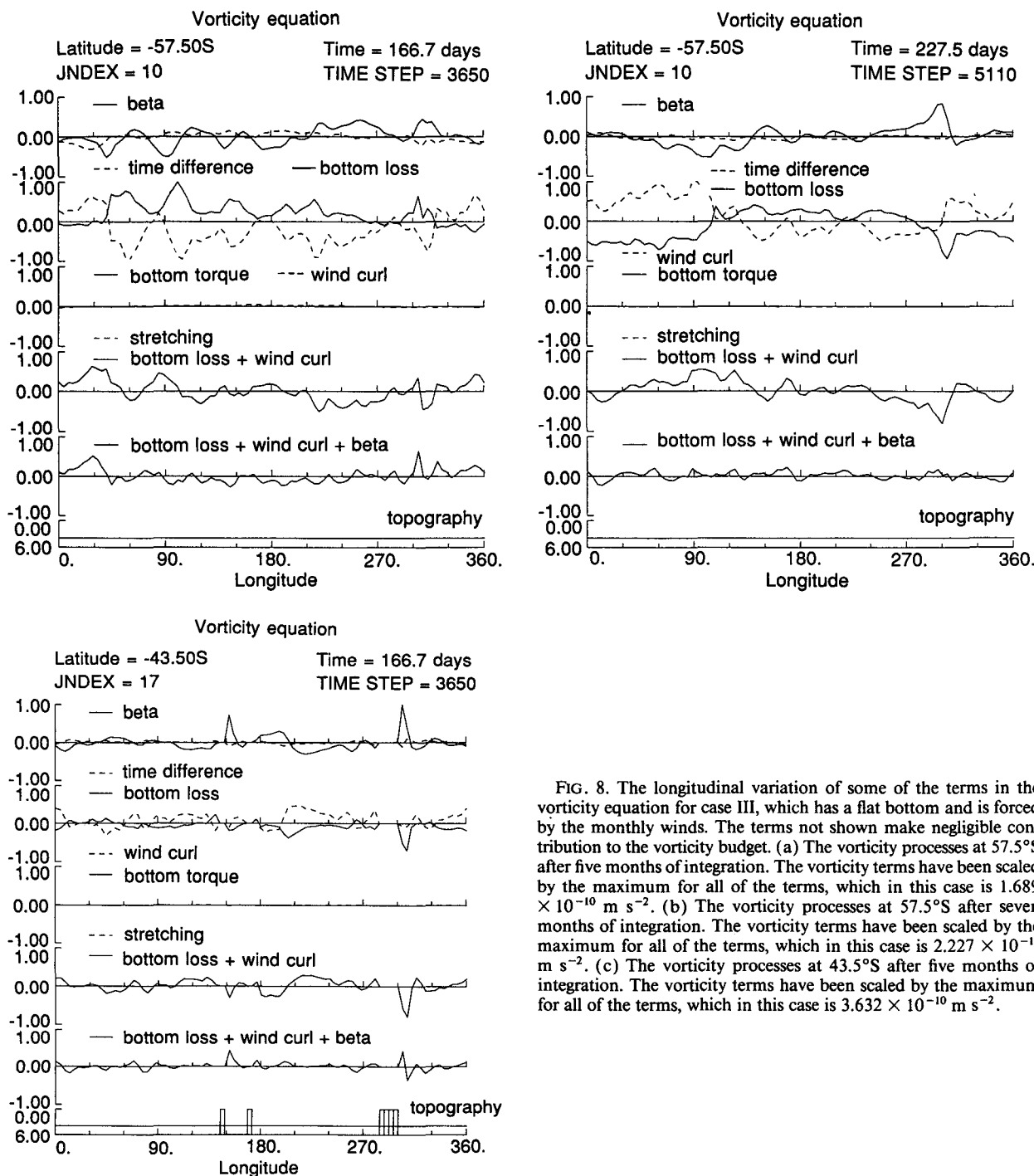

FIG. 8. The longitudinal variation of some of the terms in the vorticity equation for case III, which has a flat bottom and is forced by the monthly winds. The terms not shown make negligible contribution to the vorticity budget. (a) The vorticity processes at 57.5°S after five months of integration. The vorticity terms have been scaled by the maximum for all of the terms, which in this case is 1.689 $\times 10^{-10}$ m s^{-2}. (b) The vorticity processes at 57.5°S after seven months of integration. The vorticity terms have been scaled by the maximum for all of the terms, which in this case is 2.227 $\times 10^{-10}$ m s^{-2}. (c) The vorticity processes at 43.5°S after five months of integration. The vorticity terms have been scaled by the maximum for all of the terms, which in this case is 3.632 $\times 10^{-10}$ m s^{-2}.

action between wind curl and beta. The balance in the Atlantic sector is still developing so the time derivative term is appreciable. In fact, the Atlantic sector is being forced directly; wind curl is directly producing relative vorticity and the beta and bottom loss terms are quite small. Time changes are an important part of the overall balance, but the major processes are wind curl, beta, and bottom loss.

After seven months (Fig. 8b), the winds are at a maximum and the flow has accelerated; although it is not changing much at this time, as indicated by the small time-difference term. The wind curl in the Atlantic sector is quite large while that in the Pacific and Indian sectors is smaller in amplitude, but still negative. Wind curl and bottom loss balance; however, the Sverdrup balance is important in the Indian Ocean and in the eastern Pacific Ocean. Beta and bottom loss are the largest terms in the Scotia Sea.

At the blocked latitude (43.5°S) after five months (Fig. 8c), wind curl and bottom loss are opposite and there is a Sverdrup balance in the Pacific sector. The western boundary balance is clearly indicated on the coast of South America, and less clearly shown on Australia and New Zealand. The time variability at this latitude is quite small in contrast to that at the same time in the unblocked latitude (Fig. 8a).

d. Case IV: Bottom topography with zonally averaged monthly wind stress

This case is different from case I only in that the full bottom topography of the Southern Ocean (Fig. 1) is included. All of the parameters are the same as case I and the circulation is forced by the zonal average of the monthly wind stress. This case was run for two years to ensure decay of initial transients; the second year of the simulation is analyzed.

The transport through Drake Passage (Fig. 9a) ranges between 10 and 25 Sv and has more of an annual time variation as compared to the flat bottom simulations. The surface elevation at the Greenwich meridian (Fig. 9b) indicates that there are two separate currents: one at about 45°S with a surface difference of about 4 cm and one at about 58°S with a surface difference of about 3 cm. The northern core varies only slightly in response to the subtropical gyres while the southern core has a stronger semiannual variability. The surface elevation in Drake Passage (Fig. 9c) is rather steady with an elevation change of about 8 cm. The surface slope in the northern part of the passage changes with an annual period, while that in the southern passage has a smaller amplitude semiannual variation. The two cores in the central Atlantic (Fig. 9b) are two branches of the current that flows through Drake Passage.

The vorticity processes for this case are completely different from those in the constant depth simulations.

After five months of integration at 57.5°S (Fig. 10a), the largest values in the vorticity equation occur in the Scotia Sea. The wind curl is quite small in comparison but it is the cumulative effect of the wind that is driving the circulation. First of all, dissipation along this lati-
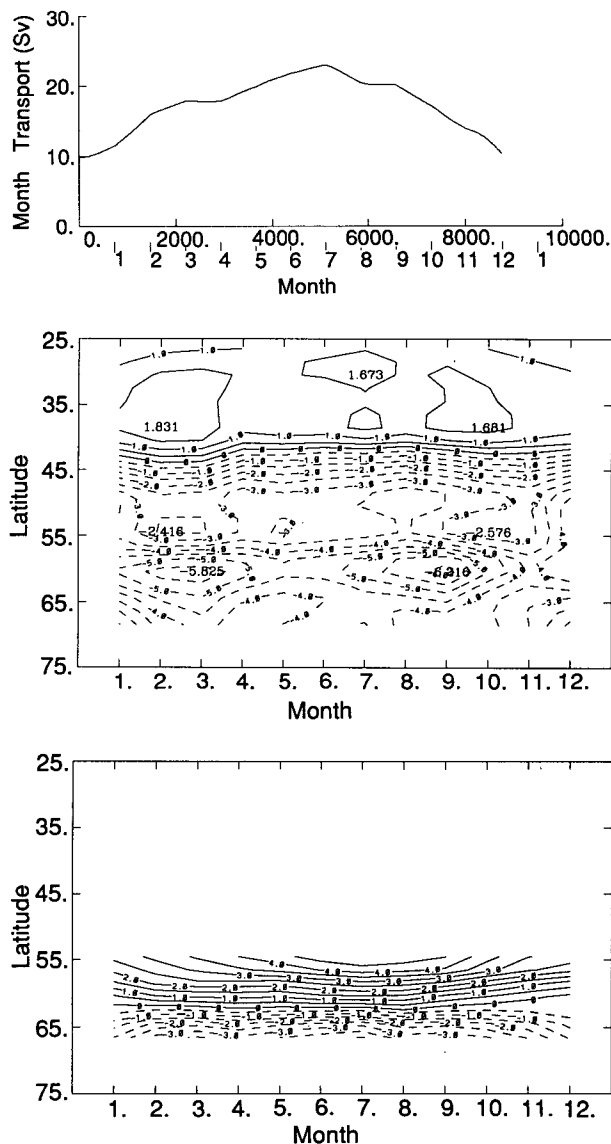

FIG. 9. Total transport and surface elevation changes for case IV, which has bottom topography and is forced by the zonal average of the monthly winds. The simulation begins at a state of rest. (a) The total transport for the first year of the simulation as a function of time. Both time step and month are indicated. The monthly tics indicate the beginning of the month. The ordinate has units of 1 Sv = 1 × 10⁶ m³ s⁻¹. (b) The variation of the surface elevation (cm) at the Greenwich meridian by month on the abscissa and latitude on the ordinate. The contour interval is 0.5 cm and the maximum values are marked. Dashed lines indicate negative values. (c) The variation of the surface elevation (cm) across Drake Passage by month on the abscissa and latitude on the ordinate. The contour interval is 0.5 cm. Dashed lines indicate negative values.
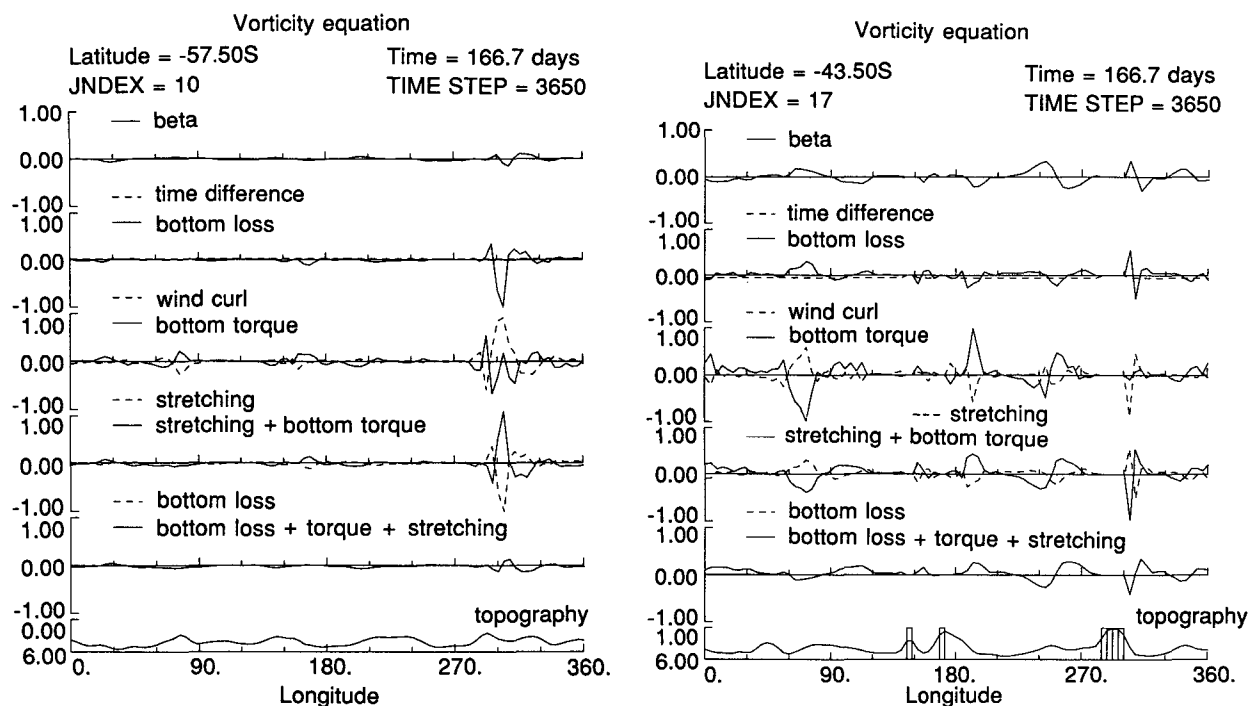
FIG. 10. The longitudinal variation of some of the terms in the vorticity equation for case IV, which has a flat bottom and is forced by the zonal average of the monthly winds. The terms not shown make negligible contribution to the vorticity budget. (a) The vorticity processes at 57.5°S after five months of integration. The vorticity terms have been scaled by the maximum for all of the terms, which in this case is 4.289×10^{-9} m s^{-2}. (b) The vorticity processes at 57.5°S after seven months of integration. The vorticity terms have been scaled by the maximum for all of the terms, which in this case is 1.164×10^{-9} m s^{-2}.

tude occurs almost exclusively in the Drake Passage–Scotia Sea area.

Two other large terms are stretching and bottom torque (third panel) and these terms mainly cancel. There are three regions where these two terms are large: Drake Passage–Scotia Sea (300° to 320°), Kerguelen Plateau (70°), and Campbell Plateau (170°)—the major topographic features along this latitude. There is very little activity over the East Pacific Rise but the ACC turns north along the rise at this latitude so there is very small interaction with the bottom. The reason for this difference in behavior is evident from the distribution of f/h (Koblinsky 1990). Near the East Pacific Rise, the planetary vorticity isopleths are continuous through the South Pacific over the rise allowing the current to conserve potential vorticity. The three areas mentioned above are locations where the planetary vorticity isopleths either end on land masses or change direction quickly (recall that the radius of deformation is a limit on the radius of curvature of the flow, in this case 2000 km) and must activate other vorticity processes to negotiate the bathymetry.

It is clear from the fourth panel that the sum of stretching and bottom torque largely cancel; the net effect of stretching and bottom torque is to produce relative vorticity, which is removed by bottom friction. It will be shown below that the vorticity process rep-

resented by the sum of stretching and bottom torque is that the flow is driven across lines of constant planetary vorticity (f/h) and, in doing so, relative vorticity is created to conserve potential vorticity. The residual of the sum of stretching, bottom torque, and bottom loss (fifth panel) is balanced by beta, which has a minor role except where the flow is driven across the latitude line by the bottom topography or in the western boundary current on South America. Similar vorticity interactions occur at other times so the figures will not be shown.

Nearly identical processes occur at the blocked latitude (43.5°S) after five months of integration (Fig. 10b) although the individual vorticity terms are more nearly the same size. The wind curl term is larger at this latitude but it is still small compared to the other terms. As in the unblocked latitude, the largest terms are stretching and bottom torque (third panel), and the sum of these two terms is strongly anticorrelated with bottom loss. The interplay of these three terms is that relative vorticity is created when the flow is forced across planetary vorticity isopleths and the resulting relative vorticity is removed by bottom friction. The residual of the sum of all three of these terms (fifth panel) is balanced by beta (first panel), which represents flow being forced across latitude lines by the topography.

e. Case V: Bottom topography with zonally averaged anomaly wind stress

This final case is different from case II only in that the bathymetry of the Southern Ocean (Fig. 1) is included. All of the parameters are the same as case II and the circulation is driven by the zonal average of the monthly wind stress anomaly from the annual mean. As with case IV, this simulation was run for two years and the second year is analyzed.

The transport at Drake Passage (Fig. 11a) ranges from −8 to 5 Sv with a predominantly annual period, which is the same range and character of variation as given for case IV (Fig. 9a). The surface elevation at Greenwich meridian (Fig. 11b) has a maximum range of about 2 cm with an annual variation north of 58°S and semiannual variation south of that latitude. The surface elevation in Drake Passage (Fig. 11c) pivots about the center of the passage with an annual period. The maximum surface difference is 1.5 cm.

The vorticity terms at 57.5°S after five months of integration (Fig. 12a) are quite similar, except smaller by a factor of six, to those of the previous case (Fig. 10a). The largest terms are in the Scotia Sea where the majority of the vorticity loss occurs. The bottom torque and stretching terms cancel (third panel) and the residual of these terms is balanced by bottom loss, principally, and to some extent by wind curl and beta. The only appreciable time derivative occurs in Drake Passage due to the developing boundary current. This case is the most complicated as several processes balance the wind curl. In the far eastern Pacific Ocean (250° to 280°), beta balances the wind curl, while farther to the east over the East Pacific Rise (210° to 240°), bottom torque counters the wind curl. South of Africa (30°), the wind curl is absorbed directly by bottom loss.

The vorticity at 57.5°S after seven months of integration (not shown) results in vorticity processes that are basically the negative of those shown in Fig. 12a. The largest terms are in the Scotia Sea area; bottom torque and stretching compensate and bottom loss removes the residual of bottom torque and stretching.

The vorticity terms at 43.5°S after five months of simulation (Fig. 12b) are complicated, but interpretable in general terms; furthermore, most of the terms are of comparable magnitude. There are only a few places where bottom loss balances wind curl (second panel, near 90°). As with the other cases with bathymetry, bottom torque and stretching balance (third panel), except in the western boundary current on South America where the two terms have the same sign. Bottom loss and the residual of bottom torque and stretching are of opposite sign (fourth panel), but bottom loss is about twice the size of the residual. Beta plays a prominent role in the vorticity balance but it does not balance any single term. The vorticity balance on the western boundary is not at all a western boundary balance, since beta and bottom loss are the same
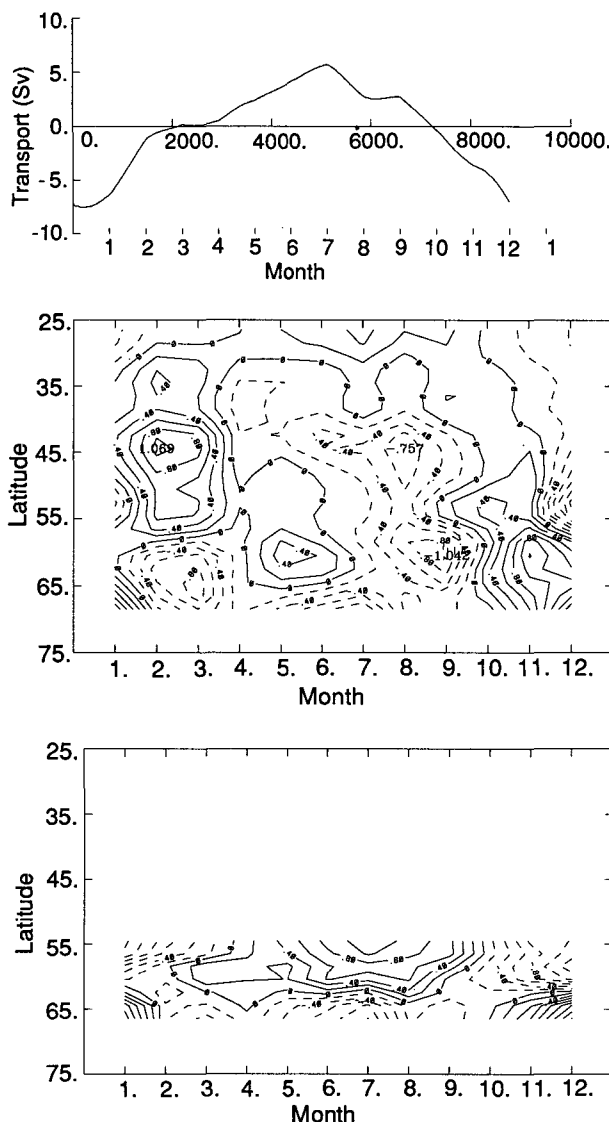

FIG. 11. Total transport and surface elevation changes for case V, which has bottom topography and is forced by the zonal average of the monthly winds minus the annual mean. The simulation begins at a state of rest. (a) The total transport for the first year of the simulation as a function of time. Both time step and month are indicated. The monthly tics indicate the beginning of the month. The ordinate has units 1 Sv = 1 × 10⁶ m³ s⁻¹. (b) The variation of the surface elevation (cm) at the Greenwich meridian by month on the abscissa and latitude on the ordinate. The contour interval is 0.2 cm and the maximum values are marked. Dashed lines indicate negative values. (c) The variation of the surface elevation (cm) across Drake Passage by month on the abscissa and latitude on the ordinate. The contour interval is 0.2 cm. Dashed lines indicate negative values.

sign (both creating negative vorticity). The bottom torque and stretching create positive vorticity as the vortex columns move into shallower water (recall that this is a time that the monthly winds are at a minimum so the anomaly winds are easterlies and the circulation is "backwards"). Both the western boundary current and the ACC are northward so beta creates negative
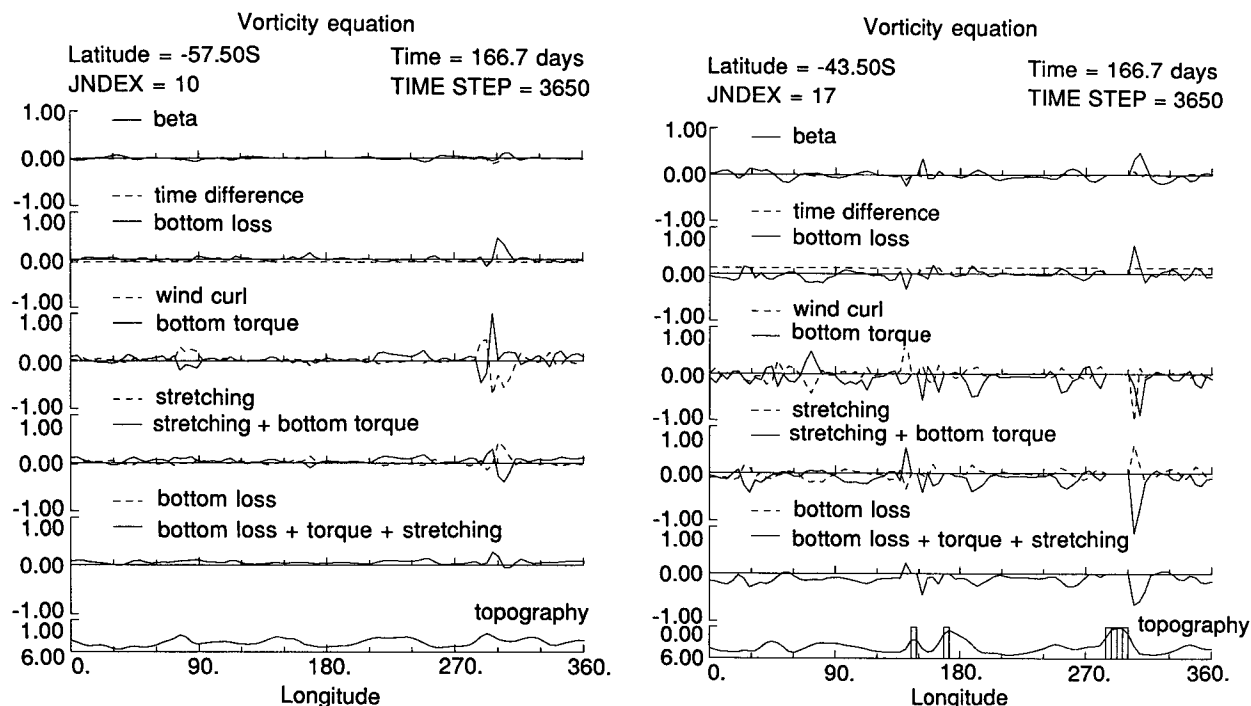
FIG. 12. The longitudinal variation of some of the terms in the vorticity equation for case V, which has bottom topography and is forced by the zonal average of the monthly winds minus the annual mean. The terms not shown make negligible contribution to the vorticity budget. (a) The vorticity processes at 57.5°S after five months of integration. The vorticity terms have been scaled by the maximum for all of the terms, which in this case is 6.307×10^{-10} m s^{-2}. (b) The vorticity processes at 43.5°S after five months of integration. The vorticity terms have been scaled by the maximum for all of the terms, which in this case is 2.247×10^{-10} m s^{-2}.

vorticity, which balances that produced by the bottom interaction. The excess positive vorticity is then removed by bottom loss.

Because of the number of simultaneous processes occurring in this simulation, it is not worthwhile to analyze the interactions in terms of two process balances. The circulation is driven by the wind forcing; and where possible—that is, if the bottom topography and coastal geometry allows it—the vortex columns move north or south to adjust to the vorticity change. In some cases, the vortex columns are driven across planetary vorticity isopleths with the effect that relative vorticity is created and subsequently removed by bottom friction. The continental barrier of South America channels the vortex columns requiring substantial creation of relative vorticity, and hence, its removal.

4. Discussion

The implication of the vorticity calculations presented in the previous section can be understood in the context of several previous analyses of the wind driven circulation in the Southern Ocean.

a. Comparison of case I and linear ACC models

The flat bottom simulation forced by zonally averaged monthly winds (case I) is most closely related to

the analytical model of Gill (1968), which considered the steady circulation in a zonal channel with partial barriers. The drag mechanism in that study is linear bottom friction although at the end of the paper some comments are made about the importance of lateral friction.

The essence of the analysis (Gill 1968) is that the wind-forced flow in a zonal channel with partial barriers is dominated by several boundary layers. There is a western boundary layer (denoted E in Gill 1968, his Fig. 2) with a width L_S ($=r/\beta = 153$ km in this case) and a frictional layer of the same thickness (denoted F) by which flow rounds the end of the partial barrier (Drake Passage). A modified Sverdrup layer (denoted B), balancing wind curl, beta, and bottom drag, exists on the eastern side of the ocean basin, the size of which is determined by the parameter ϵ [$= L_x L_S / L_G{}^2$, where L_x is the width of the basin (23 040 km) and L_G is the width of Drake Passage (about 600 km) giving a value of 9.8 for this case]. If ϵ is much less than 1 (not the case here), then most of the central part of an ocean basin is covered with a Sverdrup balance. As ϵ is equal to or greater than 1, the area having a Sverdrup balance is more strongly confined to the northeastern corner of the ocean basin. There are two other frictional boundary layers with thicknesses given by $\sqrt{\epsilon}$ (=3.8 for this case). One of these layers (denoted A) exists

along the northwestern corner of the basin, decreasing in thickness to the east; the other (denoted C) extends into the ocean from the end of the partial barrier, thickening to the west. The second boundary layer couples frictionally the flow in the unblocked zonal channel with that in the blocked part of the model. For the parameter values considered here, this layer should have a maximum thickness of about $4L_G$, which is about 2400 km. A final subdomain in the Gill model (denoted D) is an unblocked zonal channel, which is directly forced by the wind stress and damped by bottom friction.

The nondimensional scales for case I reveal that the majority of the interior of the model should be dominated by the frictional boundary layer emanating from the end of the partial barriers and that the Sverdrup balance should hold only over a small part of the model (the northeastern corner of each basin). However, there will be a western boundary layer with a width of L_S on each of the walls. Furthermore, a frictional layer exists around the end of South America with the same thickness. This boundary layer explains the appearance of a "western boundary" vorticity balance in the center of Drake Passage (e.g., Fig. 4a).

A second result from Gill (1968) is that the zonal current should thicken to the west of any partial barrier. The combined width of the ACC and the southern limb of the subtropical gyre in the central Atlantic is about 20° of latitude (Fig. 3b), which is about 2200 km and corresponds to the current width ($\sqrt{\epsilon}L_G \sim 2400$ km) estimated by Gill (1968). The location of this boundary layer also determines the location of the ACC as the latitude of the tip of South America rather than at the zero of the wind curl. The subtropical gyres are bounded by the zero curl line, which is a few degrees north of the tip of South America; this displacement is the likely explanation for the existence of the Falklands (Malvinas) Current.

b. The effect of mean flow: Cases I and II

Given the large grid spacing and slow speed for the flow, there is very little interaction of the mean flow with the seasonally varying flow. This is evident from the variation about the mean in Fig. 3 and comparing the result to Fig. 5. Although the initial transients (first 1.5 months) are different, the remainder of the transport and surface elevation variations compare closely. The vorticity calculations (Figs. 4 and 6) lead to similar conclusions about which processes are important. The time-mean circulation (Fig. 4) produces vorticity effects so large that the seasonal changes are hard to see in case I but are clearer in case II (there is a factor of ten difference in the scale for the two figures). Because of the smaller values in case II, the errors in the vorticity calculation are somewhat larger. Nevertheless, the interpretation of the two cases is essentially the same.

c. The effect of zonally varying forcing: Cases II and III

The importance of the nonzonal structure of the wind on the circulation in the Southern Ocean is seen by comparing cases II and III. In terms of the transport at Drake Passage, there is almost no difference between these two cases. The general structure of the surface elevation in Drake Passage is nearly identical (Figs. 5c and 7c) but on the Greenwich meridian (Figs. 5b and 7b) the solutions are noticeably different in character, although the peak values of surface elevation are comparable. The biggest difference is in the structure of the Weddell gyre centered on 65°S.

The most pronounced difference between the two cases is evident in the vorticity figures (Figs. 6 and 8). The first difference is that the vorticity terms in case III are about twice as large as for case I. The second difference is that the spatial variability of the forcing requires more time changes, which are Rossby waves by which the effects of the forcing are propagated to other parts of the domain. A third difference is that there are places where strong forcing directly creates relative vorticity, such as between 0° and 60°, in Fig. 8a. The wind does play a role in the structure of the circulation, but the total transport is not strongly sensitive to the nonzonal nature of the wind field. The most important role of wind variability is likely to be the creation of strong local gyres and in perturbing the flow and setting off instability for models that allow instabilities to occur.

d. Interpretation of bottom torque and stretching terms

The bottom torque and stretching terms are extracted from (6) and given below:

$$gJ(h, \eta) + f\nabla \cdot (h\mathbf{u}),   \qquad (7)$$

where $\mathbf{u} = (u, v)$ the horizontal component of the velocity vector. Under the mild condition that the flow is in geostrophic balance, the surface elevation is proportional to the geostrophic streamfunction. The geostrophic balance is well satisfied for these simulations given the slow variation of the forcing. A separate calculation of the momentum budget (not shown) found that the departures from geostrophic balance were at most a few percent of the magnitude of the Coriolis term.

Under the geostrophic assumption, the first term in (7) can be written as

$$-f\mathbf{u} \cdot \nabla h,   \qquad (8)$$

which is nonzero if the geostrophic flow crosses topographic contours. The second term in (7) is simply the effect of changing the length of a vortex tube if there is a divergence of the depth-integrated transport. Using (8) in place of the Jacobian term, (7) reduces to

$$fh\nabla \cdot \mathbf{u}. \qquad (9)$$

The net effect of bottom torque and stretching is related to the divergence of the depth-averaged flow. So this net effect is expected to be largest in divergent regions, such as the Scotia Sea where the flow spreads after passing through the narrow Drake Passage (Fig. 10a, fourth panel).

e. Case IV and numerical models with variable bottom topography

There are a number of studies of the effect of bottom topography on zonal jets (e.g., Pratt 1989; Hogg 1980) but these are difficult to compare to the present Southern Ocean model because these analytical models require simplified forms for the initial currents or bottom topography. Earlier studies of the ACC using one-layer models indicate that bottom topography produces a large drag. Schulman (1975) used a one-layer numerical model of the Southern Ocean having South America and the Antarctic penninsula as land boundaries and including the bathymetry from Drake Passage, the inclusion of which reduced the total wind-driven transport from 195 Sv to 20 Sv (same as the results obtained here). Munk and Palmén (1951) estimated that form drag on the four largest topographic features in the Southern Ocean can balance a surface wind stress of 0.2 N m^{-2} if there is a net pressure difference across the topography of about 0.04 dyn m. These pressure differences are quite small compared to the pressure change across the ACC of more than 1 dyn m (Gordon et al. 1978).

It is worth mentioning at this point that viscous dissipation is less important in determining the transport in one-layer models with bathymetry. The form drag is the major drag mechanism while friction controls the adjustment time and the width of the currents. There has not been a thorough study of this issue but the comparable transport change in this model and Schulman (1975) illustrates the effect.

A recent paper (Johnson and Bryden 1989) examines the effect of bottom drag but does so in a baroclinic context including the effect of mesoscale eddies, neither of which are present in this model. Treguier and McWilliams (1990) analyze an eddy-resolving calculation in a zonal channel with topography to find that stationary topographic eddies result in distortions of isopycnals that lead to form drag similar to bathymetric form drag. Both of these mesoscale eddy effects are likely to be important for dissipation over a long time (of order years), but the role of these eddy dissipation effects on seasonal changes is not clear. That is, does the level of eddy activity change rapidly enough to respond to seasonal wind changes?

The inclusion of bottom topography in the current model has a large effect on the solution. The mean transport is reduced by a factor of 10 (Fig. 3a compared

to Fig. 9a) while the range of transport variations are reduced by a factor of 5 (Fig. 5a compared to Fig. 10a). These results are expected from the previous analyses.

The reduction of the transport of the ACC by bottom topography is typically ascribed by these studies to bottom form drag, which is due to a pressure difference across a topographic feature. An analysis of the vorticity interactions in the present model indicates that the effect of topography occurs in two steps. As a current crosses isobaths due either to forcing or to the requirement that flow move from one deep basin to another, bottom torque creates relative vorticity, and various vorticity interactions come into play. In these simulations, the stretching term nearly always opposed the bottom torque, which leads to the interpretation that as the geostrophic flow is driven across topographic contours, the vortex lines change in length producing relative vorticity. The ultimate fate of this vorticity is to be removed by the linear (bottom) loss in the model. In a less viscous calculation, this relative vorticity may propagate as Rossby waves or trigger eddy creation. The largest vorticity processes for the simulations discussed here occur in Drake Passage because the ACC must go through this region; so production of relative vorticity by stretching and removal by friction must occur. There is a global balance that occurs when the removal of vorticity at Drake Passage is balanced by the addition of vorticity by the wind curl over the rest of the Southern Ocean. This interpretation is analogous to the porous plug idea advanced by Stommel (1962) in which all of the dissipation in the Southern Ocean occurs in Drake Passage.

5. Summary

The purpose of this paper is to consider the vorticity dynamics of the seasonal changes of the circulation in the Southern Ocean. Five simulations are studied that identify the influence of bathymetry, mean flow, and nonzonal structure of the monthly varying winds.

The time character of the simulated transport of the ACC compares in general with that measured at Drake Passage (Whitworth and Peterson 1985). The amplitude of the mean transport from the model is twice the measured value for flat bottom simulations and it is about 20% of the measured value for simulations with bathymetry. The seasonal variation in the simulated transport is almost correct for the flat bottom case with zonally averaged winds (case II, Fig. 5a), about twice the measured variation for the flat bottom case with monthly anomaly winds (case III, Fig. 7a), and about one-quarter of the measured variation for the case with bathymetry (case V, Fig. 11a). One of the limitations of this study is the large value of friction, so future simulations will have smaller grid spacing with smaller

friction coefficients, thus allowing consideration of the importance of friction on the conclusions reached here.

A general conclusion from this study is that the Sverdrup balance is not a significant two-term vorticity balance in the Southern Ocean, a result that has been shown theoretically by Clarke (1982). However, Wyrtki (1960), Baker (1982), and Godfrey (1989) each find that the amount of water driven across the latitude of the tip of South America by the curl of the wind stress (the Sverdrup transport) corresponds to the total transport measured in Drake Passage. Furthermore, the dynamic height relative to 4000 m has the same longitudinal dependence as that predicted by the wind curl estimate (Fig. 3 in Baker 1982). Peterson (1988) analyzed the time behavior of the bottom pressure at the north and south sides of Drake Passage and compared these to the zonally averaged wind stress curl over narrow latitude bands, which were on either side of the ACC. He found that the pressure changes were consistent with Sverdrup forcing by the average wind stress curl. It is unclear whether these transport and pressure estimates are similar to the Sverdrup transport by coincidence or if the integral of the Sverdrup balance is a robust estimator of the total transport independent of the detailed dynamics of the current. This last possibility is doubtful since the transport obtained from the model is quite different in cases II and IV so that the bottom topography must play a major role in the dynamics. However, the role of stratification has yet to be investigated in detail to see how it bears on the applicability of a Sverdrup balance. The resolution of this issue will require the careful analysis of more realistic model calculations.

a. Conclusions from the flat bottom simulations

The solutions discussed here are time-dependent versions of the Gill (1968) steady model; but, the model remains in quasi-equilibrium. The various boundary layers identified by Gill are present in the solutions and the thicknesses of the layers agree with the scaling from Gill.

The latitude of the end of the partial barrier (South America) controls the location of the ACC, if there is no bathymetry. The zero of the wind stress curl determines the place where the partial western boundary layer leaves the coast.

Partial barriers allow transport of vorticity across lines of zero of the wind curl even for a linear simulation.

The mean circulation is balanced by dissipation in Drake Passage while the seasonally varying circulation is balanced by dissipation throughout the Southern Ocean.

The character of the pressure changes in Drake Passage is reproduced by the model; surface elevation variations occur in the southern passage and only small changes occur in the northern passage.

In the zonal part of the flat bottom simulation, the vorticity balance is basically that of a zonal channel in which the curl of the surface stress is balanced by the curl of the bottom stress. There is, however, a place, Drake Passage, where relative vorticity is created (and removed) as in a classical western boundary. This balance, which is not expected in a purely zonal channel, is due to a boundary layer that exists around the tip of South America. This frictional layer plays an active role in removing vorticity that has been added to the ocean by the wind curl; that is, there is enhanced removal of vorticity in the narrow part of the Southern Ocean merely because of the nearby continental boundary. Therefore, even the unblocked part of the Southern Ocean does not act strictly like a zonal channel. It remains to be seen if the lower friction simulations (for which the frictional layer is more confined to the land) give rise to a different character to the zonal vorticity balance.

b. Conclusions from the variable bottom topography simulations

The magnitude of the friction parameter influences the width of the currents and the development time, but it has a weak influence on the location of the ACC and the transport.

There is a very different balance for the cases with variable bottom topography. For these cases, the largest loss of vorticity occurs in the vicinity of Drake Passage, and the vorticity balance involves three terms. Water is forced to flow through Drake Passage and over the Scotia Arc, east of Drake Passage, and is shallower than the basins on either side, so the vortex lines are required to shrink as they enter the passage. The shrinking requires relative vorticity to be created since the vortex lines are not allowed to move north or south because of the continental boundaries. Relative vorticity is then removed by bottom friction. There is some drag on the flow at other places around the zonal channel, but the largest drag is clearly in the narrow and shallow part of the ocean: Drake Passage.

REFERENCES

Baker, D. J., Jr., 1982: A note on Sverdrup balance in the southern ocean. *J. Mar. Res.,* **40**(Suppl.), 21–26.
Bryan, K., and M. D. Cox, 1972: The circulation of the World Ocean: A numerical study. Part I: A homogeneous model. *J. Phys. Oceanogr.,* **2,** 319–335.
Chelton, D. B., M. G. Schlax, D. L. Witter and J. G. Richman, 1990: Geosat altimeter observations of the surface circulation of the Southern Ocean. *J. Geophys. Res.,* **95,** 17 877–17 903.
Clarke, A. J., 1982: The dynamics of large-scale, wind-driven vari-

ations in the Antarctic Circumpolar Current. *J. Phys. Oceanogr.,* **12,** 1092–1105.

Gates, W. L., and A. B. Nelson, 1975: A new (revised) tabulation of the Scripps topography on a 1° global grid. Part II: Ocean depths, R-1277-1-ARPA, The Rand Corporation, Santa Monica, Ca., 132 pp.

Gill, A. E., 1968: A linear model of the Antarctic Circumpolar Current. *J. Fluid Mech.,* **32,** 465–488.

——, 1982: *Atmosphere-Ocean Dynamics.* Academic Press, 662 pp.

Godfrey, J. S., 1989: A Sverdrup model of the depth-integrated flow for the World Ocean allowing for island circulations. *Geophys. Astrophys. Fluid Dyn.,* **45,** 89–112.

Gordon, A. L., E. Molinelli and T. Baker, 1978: Large-scale relative dynamic topography of the Southern Ocean. *J. Geophys. Res.,* **83,** 3023–3032.

Hellerman, S., and M. Rosenstein, 1983: Normal monthly wind stress over the World Ocean with error estimates. *J. Phys. Oceanogr.,* **13,** 1093–1104.

Hogg, N. G., 1980: Effects of bottom topography on ocean currents. *Orographic Effects in Planetary Flows,* edited by GARP Joint Scientific Committee, Garp Publication Series, No. 23, 169–205.

Johnson, G. C., and H. L. Bryden, 1989: On the size of the Antarctic Circumpolar Current. *Deep-Sea Res.,* **36,** 39–53.

Joyce, T. M., 1977: A note on the lateral mixing of water masses. *J. Phys. Oceanogr.,* **7,** 626–629.

Koblinsky, C. J., 1990: The global distribution of f/H and the barotropic response of the ocean. *J. Geophys. Res.,* **95,** 3213–3218.

Large, W. G., and H. van Loon, 1989: Large scale, low frequency variability of the 1979 FGGE surface buoy drifts and wind over the Southern Hemisphere. *J. Phys. Oceanogr.,* **19,** 216–232.

Leendertse, J. J., 1967: Aspects of a computational model for long period water-wave propagation, Memo. RM-5294-PR, The Rand Corporation, Santa Monica, Ca., 165 pp.

McWilliams, J. C., W. R. Holland and J. H. S. Chow, 1978: A description of numerical antarctic circumpolar currents. *Dyn. Atmos. Oceans,* **2,** 213–291.

Mesinger, F., and A. Arakawa, 1976: *Numerical Methods Used in Atmospheric Models, Vol. I, Global Atmospheric Research Programme.* GARP Pub. Series No. 17, 65 pp.

Munk, W. H., and E. Palmén, 1951: Note on the dynamics of the Antarctic Circumpolar Current. *Tellus,* **3,** 53–56.

Nowlin, W. D., Jr., and J. M. Klinck, 1986: The physics of the Antarctic Circumpolar Current. *Rev. Geophys. Space Phys.,* **24,** 469–491.

Peterson, R. G., 1988: On the transport of the Antarctic Circumpolar Current through Drake Passage and its relation to wind. *J. Geophys. Res.,* **93,** 13 993–14 004.

Pratt, L. J., 1989: Critical control of zonal jets by bottom topography. *J. Mar. Res.,* **47,** 111–130.

Schulman, E. E., 1975: A study of topographic effects. *Numerical Models of Ocean Circulation,* edited by National Academy of Sciences, National Academy of Sciences, Washington, D.C., 147–167.

Stommel, H., 1962: An analogy to the Antarctic Circumpolar Current. *J. Mar. Res.,* **20,** 92–96.

Treguier, A. M., and J. C. McWilliams, 1990: Topographic influences on wind-driven, stratified flow in a β-plane channel: An idealized model for the Antarctic Circumpolar Current. *J. Phys. Oceanogr.,* **20,** 321–343.

Trenberth, K. E., J. G. Olson and W. G. Large, 1989: A global ocean wind stress climatology based on ECMWF analyses. National Center for Atmospheric Research, NCAR/TN-338+STR, 93 pp.

van Loon, H., 1971: The half-yearly variation of the circumpolar surface drift in the Southern Hemisphere. *Tellus,* **23,** 511–516.

Whitworth, T., III, 1983: Monitoring the transport of the Antarctic Circumpolar Current at Drake Passage. *J. Phys. Oceanogr.,* **13,** 2045–2057.

——, and R. G. Peterson, 1985: Volume transport of the Antarctic Circumpolar Current from bottom pressure measurements. *J. Phys. Oceanogr.,* **15,** 810–816.

Wolff, J. O., and D. J. Olbers, 1989: The dynamical balance of the Antarctic Circumpolar Current studied with an eddy-resolving quasigeostrophic model. *Mesoscale-Synoptic Coherent Structures in Geophysical Turbulence,* J. C. J. Nihoul, Ed., Elsevier, 435–458.

Wyrtki, K., 1960: The Antarctic Circumpolar Current and the Antarctic Polar Front. *Dtsch. Hydrogr. Z.,* **3,** 153–173.